The International Journal Of Engineering And Science (IJES)
|| Volume || 5 || Issue || 12 || Pages || PP 71-83 || 2016 ||
ISSN (e): 2319 – 1813 ISSN (p): 2319 – 1805

Nonlinear State Space Modeling and Control of a Shape Memory Alloy Spring Actuator

Reza Abiri[1], Iman Kardan[2], Reza Nadafi[3], Mansour Kabganian[4]
[1]*Department of Mechanical, Aerospace and Biomedical Engineering, University of Tennessee, Knoxville, TN 37996 USA*
[2]*Department of Mechanical Engineering, University of Ferdowsi, Mashhad, Iran*
[3]*Department of Mechanical Engineering, Amirkabir University of Technology, Tehran, Iran*
[4] *Space Science and Technology, Amirkabir University of Technology, Tehran, Iran*

----------ABSTRACT----------
In this paper, a new state-space model is developed for shape memory alloy (SMA) springs which remarkably captures their nonlinear behavior during phase transformation. The validity of the proposed model is verified by multiple open-loop experimental tests. This state-space model is then used to develop a model-based controller which adjusts the force exerted by the spring using actuating voltage in order to achieve the desired values of input force reference. It will be shown that in spite of nonlinearity of the model and hysteresis phenomenon, the perfect tracking is possible when the frequency of the input force reference is low. However, in high-frequency of input force reference, the perfect tracking is not guaranteed.
Keywords-*Micro Actuator, Shape Memory Alloy, SMA Spring, Force Control, Feedback Linearization*

Date of Submission: 12 December 2016 Date of Accepted: 25 December 2016

I. INTRODUCTION

Recently, the increasing need for performing complicated operations in micro dimensions has motivated most researches to focus on modeling and control of smart materials such as IPMCs, PZTs, and SMAs. These materials are the fundamental elements for many studies. Those are employed as actuators and sensors in many micro and smart structures. Shape memory alloys are a class of micro actuators which can remember their original shape. Characteristics such as large deformation, large output force, high energy to weight ratio, and durability make SMAs suitable in the development of SMA-actuated systems for different applications. For example, SMA actuators were employed in various micro robots such as the earthworm-like micro robot, micro-wheeled robot etc. [1-6]. SMAs were also employed with the aim of control such as the active control of space structures by Peng et al.[7]and vibration control by Saad at et al.[8]. Parameter uncertainty, low speed operation and hysteresis behavior of SMAs are the issues which make it difficult to investigate an accurate model for their behavior to be applicable in control applications.

There are many papers on modeling and control of SMA behavior. Most of the models are extended for SMA wire shape. As the result, most controllers are also designed for SMA wires. For example, Song et al. [9] applied sliding mode to control the strain in SMA wires. Teh and Featherstone [10] developed a force controller for a single wire of SMA. Moallemand Lu [11] and Moallem and Tabrizi [12] employed feedback linearization to control SMA wire actuated systems. Fuzzy logic was also utilized in designing controllers for the systems with SMA wire actuators (Nguyen and Ahn [13], Lei et al. [14], Kha and Ahn [15]). Jayender et al. [16] developed a robust controller for SMA wire based on Tanaka's model.

Few models and controllers have been developed for SMA springs. Kumon et al. [17] used a simple adaptive controller for controlling the displacement of SMA spring. Bizdoaca et al. [18] developed another controller for his SMA spring actuated system. In the modeling of SMA springs, three variables play the main roles in describing the nonlinear behavior of springs. These three major variables are: deflection (or strain), temperature (or voltage), and force (or stress). Hadi et al. [19]studied the relation among these variables and proposed a comprehensive model for SMA springs. In this paper, this model is adopted for developing a state-space form for SMA springs.

In order to make the mathematical model of SMA springs more suitable for control applications, in this paper the developed model in [19] is transformed to state-space model while the validity of developed model is verified through multiple experimental tests. Then, a feedback linearization controller is designed by using the developed state-space form and its performance is evaluated in several different simulation tests. The main contributions of this paper can be summarized as follows:

- Considering the intensive nonlinearity of equations and hysteresis phenomenon, the mathematical model of a SMA spring is decoupled and extended to be written in state-space form in order to accurately describe the phase transformations in the SMA model.
- An experimental set-up has been prepared and the final developed state-space model is validated by experimental tests. It will be discussed that the experimental tests and simulation results indicate good agreement.
- Finally, by utilizing the input-output linearization method, a feedback linearization controller for SMA spring is investigated to control the output force of a SMA spring. The performance of the developed controller will be evaluated for multiple input force references.

II. SMA SPRING MODELING

It is well-known that the efficiency of an actuator depends on the accuracy of mathematical modelling of the actuator in developing control paradigm. It is noticeable that most previous research works were carried out for one dimensional behavior of SMA. Therefore, they are applicable only for describing the nonlinear behavior of SMA wires which have one dimensional behavior. Few researches reported the behavior modeling of SMA spring. Brinson [20] elaborated the model of SMA based on separating the martensite fraction and describing the behavior of SMA by transformation equations. Liang and Rogers [21] introduced a simple model for SMA Spring which was restricted by application in vibration control. Another model was developed by Aguiar et al. [22] which was investigated by experimental tests. Kardan and Abiri et al. [23] have also developed a model for SMA springs using recurrent neural networks.

Here, we employ the model developed by Hadi et al. [19]. This model is based on Brinson's model [20] and it is combined with Liang's work to improve SMA springs modeling. The final goal of this modeling is presenting the relation among three main variables which describe the behavior of SMA: deflection (or strain), temperature (or voltage), and force (or stress). In this model the voltage and deflection are considered as inputs and the force is the output of the model. The modeling procedure consists of three main sections: phase transformation, constitutive model and heat transfer. Brinson's procedure [20] is used to deal with modeling the phase transformation section.

To analyze the model of constitutive part based on the multi-dimensional model of Liang, a one dimensional shear stress and strain relation of SMA is expressed as[19]:

$$\tau = G\,\gamma + \frac{\Omega}{\sqrt{3}}\xi + \frac{\theta_T}{\sqrt{3}}T\,, \qquad (1)$$

where, τ stands for the shear stress, G is the elastic shear modulus, γ is the strain, Ω is the phase transformation tensor which can be calculated from $\Omega = -\sqrt{3}G\gamma_1$ where γ_1 is the maximum recoverable strain, and θ_T is the thermo-elastic tensor. ξ describes the percentage of martensite in the crystal structure of the SMA spring and T presents the temperature. Moreover, the martensite fraction can be assumed as sum of two different types of twinned martensite (ξ_T) and de-twinned martensite (ξ_s):

$$\xi = \xi_s + \xi_T \qquad (2)$$

Relation among deflection (y), force (F) and de-twinned martensite fraction (ξ_s), can be expressed using the following equation [19]:

$$y = \frac{128 D_s^{\,3} N}{G r_w^{\,4}} F - \frac{2\Omega N \pi D_s^{\,2}}{\sqrt{3}G r_w}\xi_s - \frac{D_s \theta_T}{2G r_w \sqrt{3}}\mathrm{T} \qquad (3)$$

in which D_s, r_w, and N are the mean diameter of SMA spring turns, radius of spring wire, and the number of SMA spring turns respectively. Shear modulus of elasticity can be expressed as a function of shear modulus of austenite phase (G_A) and martensite phase (G_M):

$$G = G_A + \xi\,(G_M - G_A) \qquad (4)$$

Finally, to cope with modeling the heat transfer part, by employing the thermodynamic law, the thermal equation can be expressed as follows [19]:

$$m C_p \frac{dT}{dt} + m L \dot{\xi} = \frac{V^2}{R} - hA\,(T - T_\infty) \qquad (5)$$

$$R = R_A + \xi \left(R_M - R_A \right) \qquad (6)$$

where m, C_p, L, h, T_∞, and A are SMA spring mass, specific heat of SMA spring, latent heat, convectional heat coefficient, temperature of environment, and SMA spring circumferential area, respectively. V is the input voltage and R is the electrical resistance which is defined by SMA resistance in the austenite phase (R_A) and SMA resistance in martensite phase (R_M).

III. STATE-SPACE REPRESENTATION FOR OPEN LOOP SYSTEM

The mathematical model of SMA springs is transformed to sate-space form to make it more convenient for developing control algorithm. To deal with presenting the model in state-space form, the state variables and the inputs are initially chosen as follows:

$$\begin{cases} x_1 = T \\ x_2 = F \\ x_3 = \xi_s \\ x_4 = \xi_T \\ u_1 = V^2 \\ u_2 = \dot{y} \end{cases} \qquad (7)$$

x_i is the i^{th} state-space variable and u_i is the i^{th} input. By replacing these variables and considering the transformation equations developed in [20], all previous describing equations (1)-(6) will be simplified and finally the state-space forms will be developed to describe the dynamic behavior of SMA spring in different transformations. In this paper, all of the transformation equations of Brinson's model [20] are elaborated in six parts, each part describes a specific type of transformation and its dynamic is defined by a particular set of state-space equations.

Five of these six parts are shown in Figure 1. In other words, the five specified sections in Figure 1 indicate five types of transformations and the sixth part is related to those conditions in which none of the five types of transformations occur. As a result, there will be six sets of state-space equations which are defined in detail as follows. Note that the force exerted by the spring (as the second state-space variable) is taken as the output of the system in the following sections.

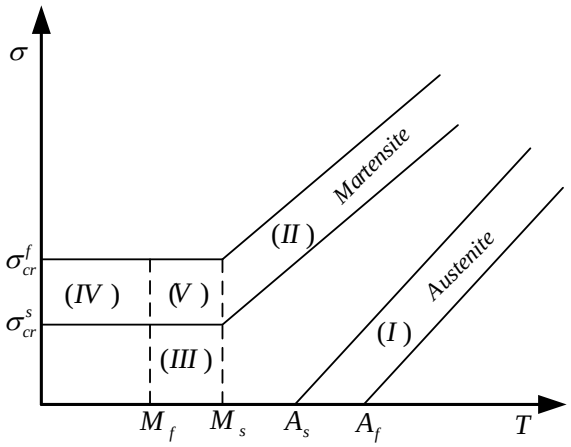

Figure 1. Schematic overview of phase diagram of shape memory alloy.

3.1. Transformation from martensite phase to austenite phase

The first section is illustrated in Figure 1. Based on Brinson's model (Brinson [20]), as the temperature of the SMA spring is increased above (Austenite start temperature), the material begins to transform to austenite phase. The transformation process continues till the spring temperature reaches Austenite finish temperature. After this temperature the material will be completely in austenite phase. As it was presented, the equations of the SMA spring model are intensive nonlinear and coupled.

In order to decouple the equations and find an explicit state-space form, some procedures and simplifications are required. By using transformation equations developed by Brinson [20], the final simplified state-space model

of the SMA spring during transformation from martensite to austenite phase can be described by the following equations:

$$\dot{T} = \dot{x}_1 = \frac{1}{m C_p}\left(\frac{u_1}{R_A + (x_3 + x_4)(R_M - R_A)} - hA(x_1 - T_\infty)\right) \quad (8)$$

$$\dot{F} = \dot{x}_2 = \frac{W}{B} \quad (9\text{-a})$$

$$W = \frac{d_w^4}{8 D_s^3 N}\left[G_A + (x_3 + x_4)(G_M - G_A)\right]u_2 + \frac{\gamma_l \pi d_w^3}{8 D_s \times 2}\left[G_A + (x_3 + x_4)(G_M - G_A)\right]\xi_s(0)\times \frac{\pi}{A_f - A_s}\times \sin\left(\frac{\pi}{A_f - A_s}\left(x_1 - A_s - x_2\frac{2R_s\sqrt{3}}{C_A \pi r_w^3}\right)\right)\dot{x}_1 + \frac{d_w^3 \pi}{8 D_s \sqrt{3}}\theta_T \dot{x}_1 \quad (9\text{-b})$$

$$B = 1 + \frac{\gamma_l \pi d_w^3}{8 D_s \times 2}\left[G_A + (x_3 + x_4)(G_M - G_A)\right]\xi_s(0)\times \frac{\pi}{A_f - A_s}\times \frac{2R_s\sqrt{3}}{C_A \pi r_w^3}\sin\left(\frac{\pi}{A_f - A_s}\left(x_1 - A_s - x_2\frac{2R_s\sqrt{3}}{C_A \pi r_w^3}\right)\right) \quad (9\text{-c})$$

$$\dot{\xi}_s = \dot{x}_3 = -\frac{\xi_s(0)}{2}\times \frac{\pi}{A_f - A_s}\times [\dot{x}_1 - \dot{x}_2\frac{2R_s\sqrt{3}}{\pi r_w^3}]\sin\left(\frac{\pi}{A_f - A_s}\left(x_1 - A_s - x_2\frac{2R_s\sqrt{3}}{C_A \pi r_w^3}\right)\right) \quad (10)$$

$$\dot{\xi} = \dot{x}_4 = -\frac{\xi_T(0)}{2}\times \frac{\pi}{A_f - A_s}\times [\dot{x}_1 - \dot{x}_2\frac{2R_s\sqrt{3}}{\pi r_w^3}]\sin\left(\frac{\pi}{A_f - A_s}\left(x_1 - A_s - x_2\frac{2R_s\sqrt{3}}{C_A \pi r_w^3}\right)\right) \quad (11)$$

where d_w, C_A, and R_s are diameter of SMA spring wire, effective coefficient of stress on austenite temperatures, and radius of SMA spring, respectively and the other parameters are defined in the previous sections.

3.2. Transformation from austenite phase to detwinned martensite phase

Section II in Figure 1 shows that if the SMA spring is cooled down from high temperatures and the applied stress is higher than (critical stress value at the start of martensitic variants conversion), the austenite phase will be directly transformed to detwinned martensite. The state equations for this transformation can be described as follows:

$$\dot{T} = \dot{x}_1 = \frac{1}{m c_p}\left(\frac{u_1}{R_A + (x_3 + x_4)(R_M - R_A)} - hA(x_1 - T_\infty)\right) \quad (12)$$

$$\dot{F} = \dot{x}_2 = \frac{W}{B} \quad (13\text{-a})$$

$$W = \frac{d_w^4}{8 D_s^3 N}\left[G_A + (x_3 + x_4)(G_M - G_A)\right]u_2 - \frac{\gamma_l \pi d_w^3}{8 D_s \times 2}\left[G_A + (x_3 + x_4)(G_M - G_A)\right](1 - \xi_s(0))\frac{\pi}{\sigma_{cr}^s - \sigma_{cr}^f}C_M \times \sin\left(\frac{\pi}{\sigma_{cr}^s - \sigma_{cr}^f}\left(x_2\frac{2R_s\sqrt{3}}{\pi r_w^3} - \sigma_{cr}^f - C_M(x_1 - M_s)\right)\right)\dot{x}_1 + \frac{d_w^3 \pi}{8 D_s \sqrt{3}}\theta_T \dot{x}_1 \quad (13\text{-b})$$

$$B = 1 - \frac{\gamma_l \pi d_w^{\ 3}}{8 D_s \times 2}\left[G_A + (x_3 + x_4)(G_M - G_A)\right](1 - \xi_s(0))\frac{\pi}{\sigma_{cr}^{s} - \sigma_{cr}^{f}} \times \frac{2R_s\sqrt{3}}{\pi r_w^{\ 3}} \sin\left(\frac{\pi}{\sigma_{cr}^{s} - \sigma_{cr}^{f}}\left(x_2 \frac{2R_s\sqrt{3}}{\pi r_w^{\ 3}} - \sigma_{cr}^{f} - C_M(x_1 - M_s)\right)\right) \quad (13\text{-c})$$

$$\dot{\xi}_s = \dot{x}_3 = -\frac{1 - \xi_s(0)}{2} \times \frac{\pi}{\sigma_{cr}^{s} - \sigma_{cr}^{f}}[-C_M \dot{x}_1 + \dot{x}_2 \frac{2R_s\sqrt{3}}{\pi r_w^{\ 3}}] \times \sin\left(\frac{\pi}{\sigma_{cr}^{s} - \sigma_{cr}^{f}}\left(x_2 \frac{2R_s\sqrt{3}}{\pi r_w^{\ 3}} - \sigma_{cr}^{f} - C_M(x_1 - M_s)\right)\right) \quad (14)$$

$$\dot{\xi}_T = \dot{x}_4 = -\frac{\xi_T(0)}{1 - \xi_s(0)}\dot{x}_3 \quad (15)$$

where C_M and σ_{cr}^{f} are effective coefficient of stress on martensite temperatures and critical stress value at the finish of the martensitic variants conversion.

3.3. Transformation from austenite to twinned martensite

SectionIIIofFigure1occurs when the SMA spring is cooled down from high temperatures and the applied stress is belowσ_{cr}^{s}, transformation from austenite to martensite starts at temperatureM_s(Martensite start temperature) and completes at M_f(Martensite finish temperature). The produced martensite phase will have multiple variants while twins will be appeared in the structure. This configuration of martensite phase is commonly called "twinned martensite" [20]. The state equations for this transformation can be described as follows:

$$\dot{T} = \dot{x}_1 = \frac{1}{m c_p}\left(\frac{u_1}{R_A + (x_3 + x_4)(R_M - R_A)} - hA(x_1 - T_\infty)\right) \quad (16)$$

$$\dot{F} = \dot{x}_2 = \frac{d_w^{\ 4}}{8 D_s^{\ 3} N}\left[G_A + (x_3 + x_4)(G_M - G_A)\right]u_2 + \frac{d_w^{\ 3}\pi}{8 D_s\sqrt{3}}\theta_T \dot{x}_1 \quad (17)$$

$$\dot{\xi}_s = \dot{x}_3 = 0 \quad (18)$$

$$\dot{\xi}_T = \dot{x}_4 = -\frac{\xi_T(0)}{1 - \xi_s(0)}\dot{x}_3 - \frac{1 - \xi_T(0)}{2} \times \frac{\pi}{M_s - M_f} \times \dot{x}_1 \times \sin\left(\frac{\pi}{M_s - M_f}(x_1 - M_f)\right) \quad (19)$$

It can be seen that $\dot{\xi}_s$ is zero because there is no change which is caused by the effect of stress during this transformation phase.

3.4. Transformation from twinned martensite to detwinned martensite

If a load is applied to the SMA spring and the stress is increased over a critical stress (σ_{cr}^{s}), the different variants will begin to reorient in the direction of the applied load. This process is called detwinning and the produced configuration is commonly called "detwinned martensite"[20].The state equations for this transformation can be simplified as follows:

$$\dot{T} = \dot{x}_1 = \frac{1}{m c_p}\left(\frac{u_1}{R_A + (x_3 + x_4)(R_M - R_A)} - hA(x_1 - T_\infty)\right) \quad (20)$$

$$\dot{F} = \dot{x}_2 = \frac{W}{B} \quad (21\text{-a})$$

$$W = \frac{d_w^{\ 4}}{8 D_s^{\ 3} N}\left[G_A + (x_3 + x_4)(G_M - G_A)\right]u_2 + \frac{d_w^{\ 3}\pi}{8 D_s\sqrt{3}}\theta_T \dot{x}_1 \quad (21\text{-b})$$

$$B = 1 - \frac{\gamma_l \pi d_w^{\ 3}}{8 D_s \times 2}\left[G_A + (x_3 + x_4)(G_M - G_A)\right](1 - \xi_s(0))\frac{\pi}{\sigma_{cr}^s - \sigma_{cr}^f} \times \frac{2R_s\sqrt{3}}{\pi r_w^{\ 3}} \times \sin\left(\frac{\pi}{\sigma_{cr}^s - \sigma_{cr}^f}\left(x_2 \frac{2R_s\sqrt{3}}{\pi r_w^{\ 3}} - \sigma_{cr}^f\right)\right) \quad (21\text{-c})$$

$$\dot{\xi}_s = \dot{x}_3 = -\frac{1 - \xi_s(0)}{2} \times \frac{\pi}{\sigma_{cr}^s - \sigma_{cr}^f} \times \dot{x}_2 \frac{2R_s\sqrt{3}}{\pi r_w^{\ 3}} \times \sin\left(\frac{\pi}{\sigma_{cr}^s - \sigma_{cr}^f}\left(x_2 \frac{2R_s\sqrt{3}}{\pi r_w^{\ 3}} - \sigma_{cr}^f\right)\right) \quad (22)$$

$$\dot{\xi}_T = \dot{x}_4 = -\frac{\xi_T(0)}{1 - \xi_s(0)}\dot{x}_3 \quad (23)$$

3.5. Section III & IV overlapped

As it is illustrated in Figure 1(section V), in this case transformations from austenite to twinned martensite and from austenite or twinned martensite to the twinned martensite occur at the same time. The state equations for this transformation can be described as follows:

$$\dot{T} = \dot{x}_1 = \frac{1}{m c_p}\left(\frac{u_1}{R_A + (x_3 + x_4)(R_M - R_A)} - hA(x_1 - T_\infty)\right) \quad (24)$$

where $\dot{x}_1$ expresses the temperature changes with respect to the other parameters and variables of the SMA spring model. Meanwhile, the following equations show the changes in the force of SMA spring:

$$\dot{F} = \dot{x}_2 = \frac{W}{B} \quad (25)$$

$$W = \frac{d_w^{\ 4}}{8 D_s^{\ 3} N}\left[G_A + (x_3 + x_4)(G_M - G_A)\right]u_2 + \frac{d_w^{\ 3}\pi}{8 D_s\sqrt{3}}\theta_T \dot{x}_1 \quad (26)$$

$$B = 1 - \frac{\gamma_l \pi d_w^{\ 3}}{8 D_s \times 2}\left[G_A + (x_3 + x_4)(G_M - G_A)\right](1 - \xi_s(0))\frac{\pi}{\sigma_{cr}^s - \sigma_{cr}^f} \times \frac{2R_s\sqrt{3}}{\pi r_w^{\ 3}} \times \sin\left(\frac{\pi}{\sigma_{cr}^s - \sigma_{cr}^f}\left(x_2 \frac{2R_s\sqrt{3}}{\pi r_w^{\ 3}} - \sigma_{cr}^f\right)\right) \quad (27)$$

$$\dot{\xi}_s = \dot{x}_3 = -\frac{1 - \xi_s(0)}{2} \times \frac{\pi}{\sigma_{cr}^s - \sigma_{cr}^f} \times \dot{x}_2 \frac{2R_s\sqrt{3}}{\pi r_w^{\ 3}} \times \sin\left(\frac{\pi}{\sigma_{cr}^s - \sigma_{cr}^f}\left(x_2 \frac{2R_s\sqrt{3}}{\pi r_w^{\ 3}} - \sigma_{cr}^f\right)\right) \quad (28)$$

$$\dot{\xi}_T = \dot{x}_4 = -\frac{\xi_T(0)}{1 - \xi_s(0)}\dot{x}_3 - \frac{1 - \xi_T(0)}{2} \times \frac{\pi}{M_s - M_f} \times \dot{x}_1 \times \sin\left(\frac{\pi}{M_s - M_f}(x_1 - M_f)\right) \quad (29)$$

3.6. No transformation happens

This part is describing the sections of Figure 1 which do not satisfy any conditions of the previous parts. In this case, no phase transformation occurs but the stress still changes gradually as a function of the temperature because of the thermal expansion effect. The state equations for this case can be described as follows:

$$\dot{T} = \dot{x}_1 = \frac{1}{m c_p}\left(\frac{u_1}{R_A + (x_3 + x_4)(R_M - R_A)} - hA(x_1 - T_\infty)\right) \quad (30)$$

$$\dot{F} = \dot{x}_2 = \frac{d_w^{\ 4}}{8 D_s^{\ 3} N}\left[G_A + (x_3 + x_4)(G_M - G_A)\right]u_2 + \frac{d_w^{\ 3}\pi}{8 D_s\sqrt{3}}\theta_T \dot{x}_1 \quad (31)$$

$$\dot{\xi}_s = \dot{x}_3 = 0 \quad (32)$$

$$\dot{\xi}_T = \dot{x}_4 = 0 \quad (33)$$

It can be seen that $\dot{\xi}_s$ and $\dot{\xi}_T$ are zero since there is no change caused by the effect of stress or temperature during this transformation.

It is clear that the equations 8-33 are complicated and intensively nonlinear. The dynamics of SMA is formed of six sets of state-space from which the assumed set is chosen by initial conditions and the rate of change of state-space variables. For any new transformation, the zero initial conditions should be replaced by the last updated condition of states.

IV. EXPERIMENTAL SET-UP

A set-up has been designed to validate the theoretical model of the SMA spring actuator which is presented in the previous section. A simple schematic of the prepared set-up has been illustrated in Figure2 and Figure3. The SMA spring used in this work is same as the one used by Hadi et al. [19]. The spring parameters are described in Table 1 in detail.

Table 1.SMA spring's coefficients used in the modeling [19]

Coefficient	Definition	Value	Unit
γ_l	Maximum shear strain	0.0567	-
Ω	Phase transformation contribution factor	$-\sqrt{3G\ \gamma_l}$	GPa
θ_T	SMA spring thermal expansion factor	0.55	MPa/°C
T_∞	Temperature of environment	23	°C
A_s	Austenite start temperature	42.6	°C
A_f	Austenite finish temperature	50.3	°C
M_s	Martensite start temperature	42.7	°C
M_f	Martensite finish temperature	36.7	°C
G_A	Shear young module in austenite	26.9	GPa
G_M	Shear young module in martensite	17	GPa
C_A	Effect of stress on austenite temperatures	6	°C
C_M	Effect of stress on martensite temperatures	12	°C
D_s	Diameter of SMA spring	6	mm
d_w	Diameter of SMA spring wire	0.75	mm
N	Number of SMA spring coils	20	-
m	SMA spring mass	0.00118	kg
C_p	Specific heat of SMA spring	350	J/kg. °C
L	Latent heat	6025	J/kg. °C
R_A	SMA resistance in austenite phase	0.7246	Ω
R_M	SMA resistance in martensite phase	0.8197	Ω
h	Convection heat coefficient	150	J/m2.
A	SMA spring circumferential area	977	mm2
σ_{cr}^{s}	Critical stress value at the start of martensitic variants	170	MPa
σ_{cr}^{f}	Critical stress value at the finish of martensitic variants	450	MPa

As it was discussed, there will be three major variables which describe the dynamic behavior of the SMA spring. The final aim is to present the relation among these three main variables: deflection (or strain), temperature (or voltage), and force (or stress). Therefore, the proposed set-up should be capable of altering and measuring these variables in order to accurately verify the nonlinear behavior of the SMA spring.

A low rpm dc motor is considered to pull the SMA spring at different speeds. Meanwhile a load cell is employed to measure the force exerted by the spring. The deflection of the spring is also measured by using a rotational potentiometer. All the measured data are transferred to PC via a data acquisition board. The third variable, voltage (temperature), is the signal command and it will be recorded in the PC automatically. Voltage is applied to the spring through the DAQ board and a current amplifier (see Figure2 and Figure3).

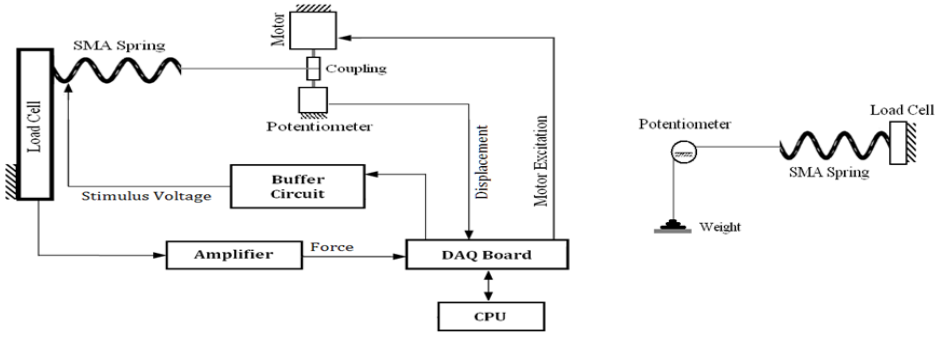

Figure 2. Schematic overview of the set-up (a): Top view with electronic circuit (Fixed voltage and fixed length tests) (b): Side view (Fixed stress tests).

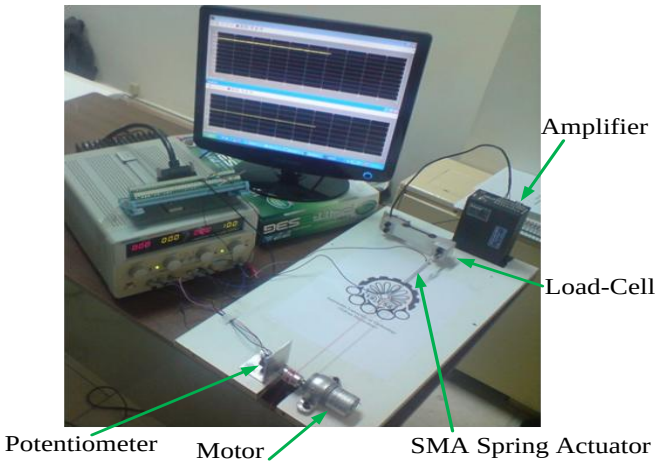

Figure 3. The single SMA spring test set-up.

The best way to find out the relation among the three mentioned variables is fixing one of the variables and considering the variation in the two other variables. In other words, three types of tests have been carried out by the proposed set-up: fixed voltage (temperature) tests, fixed length (strain) tests and fixed force (stress) tests. About 300 tests are conducted to ensure the validity of the model. As an example, a series of tests with a fixed temperature (23 °C) has been illustrated in Figure4 in which the data are raw data of the potentiometer and load cell recorded by the PC. One of these tests is separately depicted in Figure5 in comparison with simulation results. Figure 6 shows the data of another fixed temperature (90 °C) test versus simulation results.

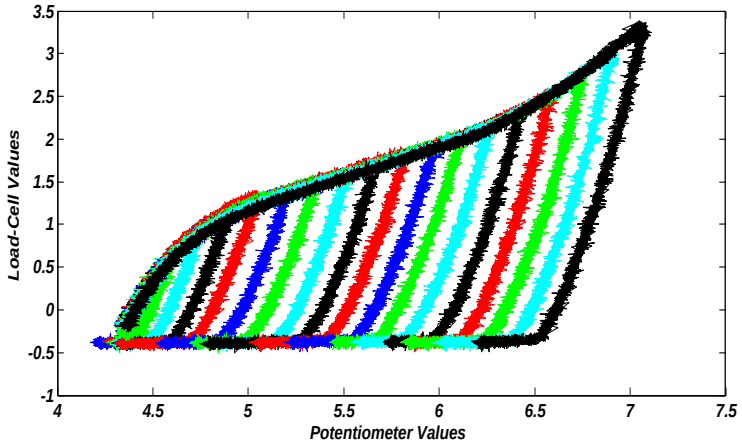

Figure 4. Raw data of potentiometer versus load cell values recorded for SMA spring in environment temperature.

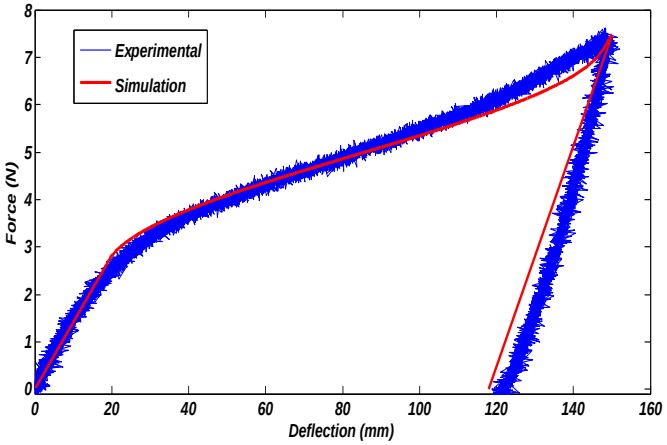

Figure 5. Force versus displacement of SMA spring in environment temperature.

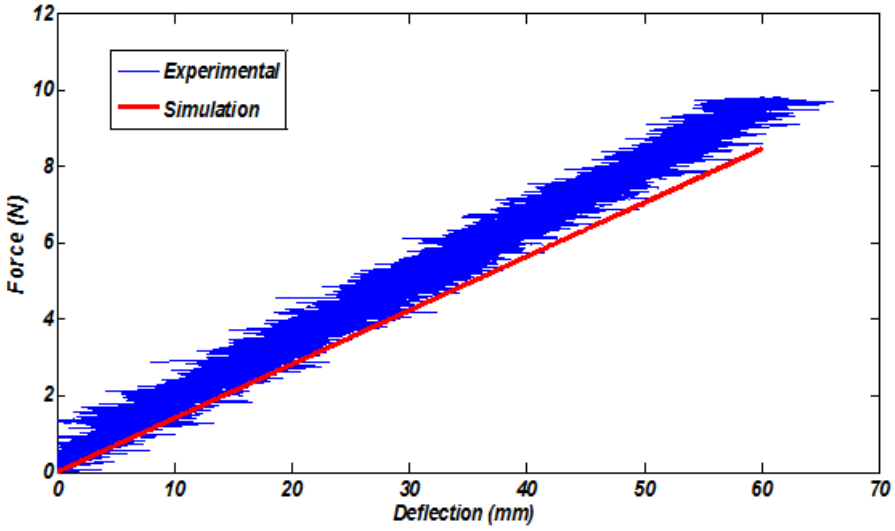

Figure 6. Elastic behavior of SMA spring in high temperature (90 °C).

Figure 5 and Figure 6 show that simulation results of developed state-space model have good agreement with the experimental tests, which confirm the validity of the proposed model.
It is clear that controlling the force exerted of an SMA spring actuator is a critical issue many applications to perform desired tasks. Furthermore, there are always uncertainties and unpredictable disturbances in systems and environments and overcoming these problems motivate the users to investigate a controllable behavior. In order to achieve these goals, designing a controller is the best way. In this paper, an advanced controller is designed to control the force exerted by the shape memory alloy spring.

V. FEEDBACK LINEARIZATION CONTROLLER DESIGN

Unrepeatable behavior of SMA and unpredictable disturbances such as change of environment temperature justifies the necessity of designing a controller. In this section, a nonlinear controller will be developed to control the output force of the system (SMA spring) in a fixed length of SMA spring. Thus, the second input of the system ($u_2 = y$) will be zero and the force of the system will be controlled by the input voltage (SISO system).
The input-output linearization method is employed to develop a control law for tracking the reference input force. By taking the first derivative of the output force $(F = x_2)$, the input will appear in the equation. Based on state-space equations the final equation can be simplified as follows:

$$\dot{x}_2 = \dot{F} = f(x) + g(x)u_1 \qquad (34)$$

where F is spring force and $f(x)$ and $g(x)$ are nonlinear functions of the state variables. It should be noted that these functions have different forms in each transformation region.Finally control law for all transformations will be defined as follows:

$$\begin{cases} u_1 = \dfrac{1}{g(x)}\left[-f(x) + r\right] \\ r = \dot{F}_d - k\left(F - F_d\right) \end{cases} \qquad (35)$$

where r is the reference signal, F_d is the desired force and k is the design coefficient which determines the speed of the response. The control law is the same for all six sets of state-spaces but its value depends on functions $f(x)$ and $g(x)$.

VI. SIMULATION RESULTS FOR CLOSED-LOOP CONTROL

All of the equations and the control law (for all different transformations) have been coded in MATLAB. To evaluate the designed controller, different desired inputs are considered. Here, we discuss a few desired inputs which lead to some prominent results.

Figure 7 shows the controlled output force versus time which is supposed to track a step input force. It illustrates satisfactory results in controlling the systems and after about seven seconds the output force will reach the step signal. Also in Figure 8, the applied voltage for controlling the SMA spring is plotted versus time. For some seconds, the system functions with a saturated voltage of 3.0 V and then it decreases to about 0.6 V.

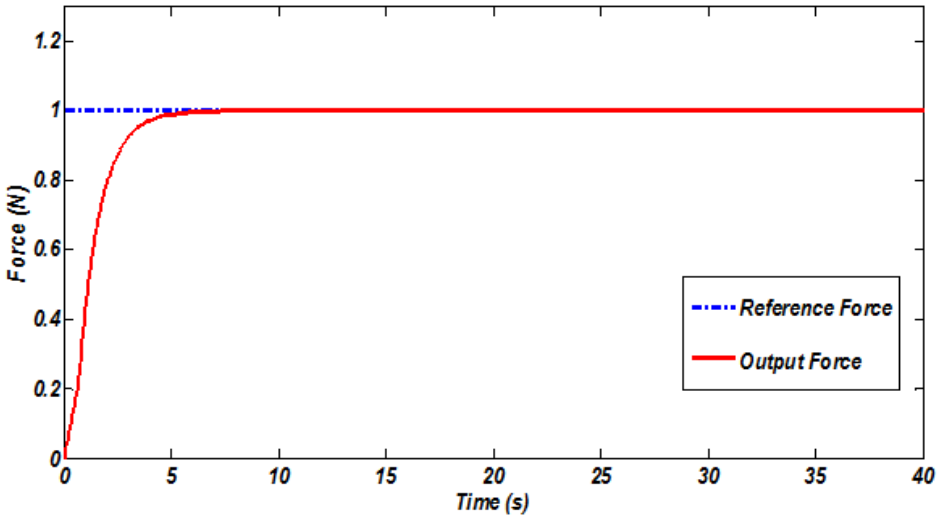

Figure 7. Controlled output force for set point input.

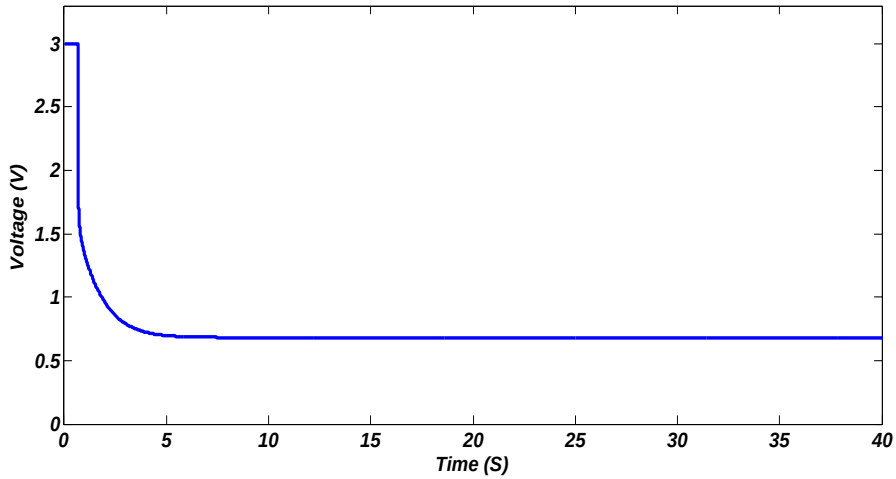

Figure 8. Actuator input voltage versus time for achieving the desired force.

Figure 9 and Figure 10 depict the tracking control result for a low frequency input (about 1.60 Hz) with low amplitude of variation of the desired force (about 1 N). It can be seen that the controller functions well and a suitable tracking is achieved. It is noticeable that for some points, the tracking is not accessible because of the low speed of cooling.

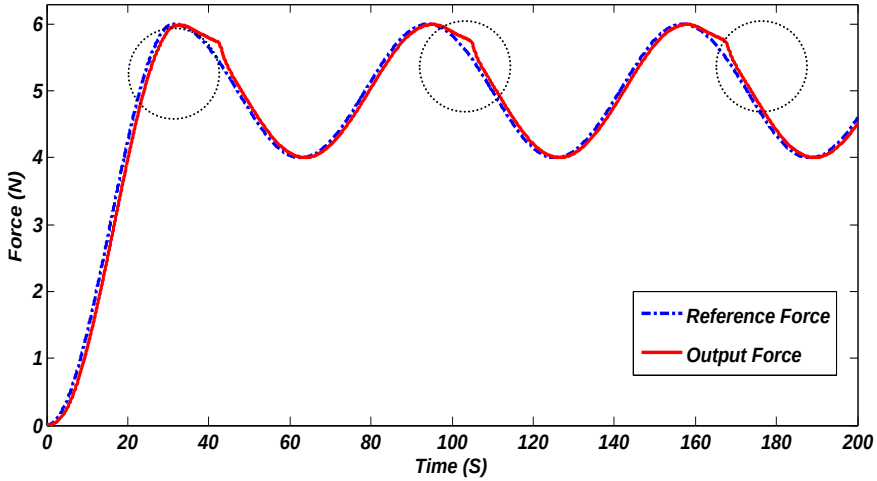

Figure 9. Tracking control result for sinusoidal input force with low frequency and small variation in amplitude.

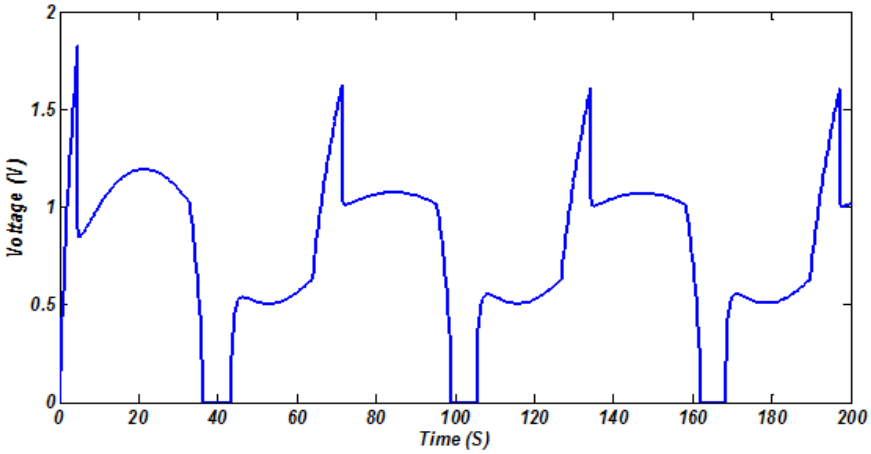

Figure10. Input voltage for tracking control in low frequency (about 1.60 Hz) and small variation in amplitude.

Figure 11 and Figure 12 illustrate the control result of SMA spring force where the reference force has low frequency but the amplitude of sinusoidal changes more (about 2N).

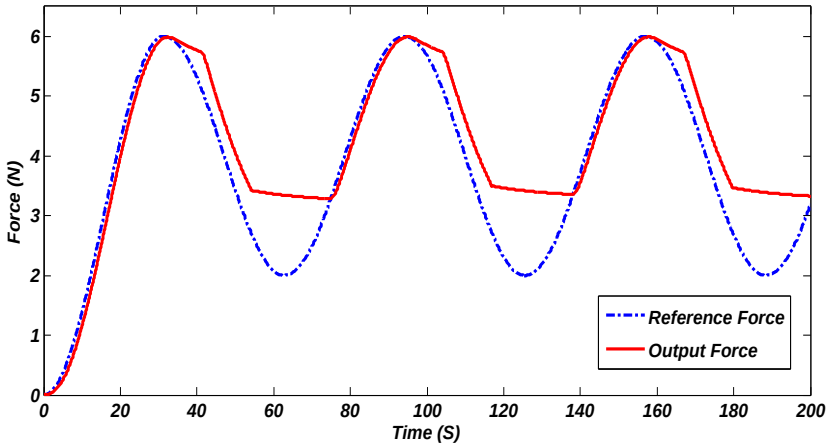

Figure 11. Tracking control for sinusoidal input force with low frequency and large high variation in amplitude.

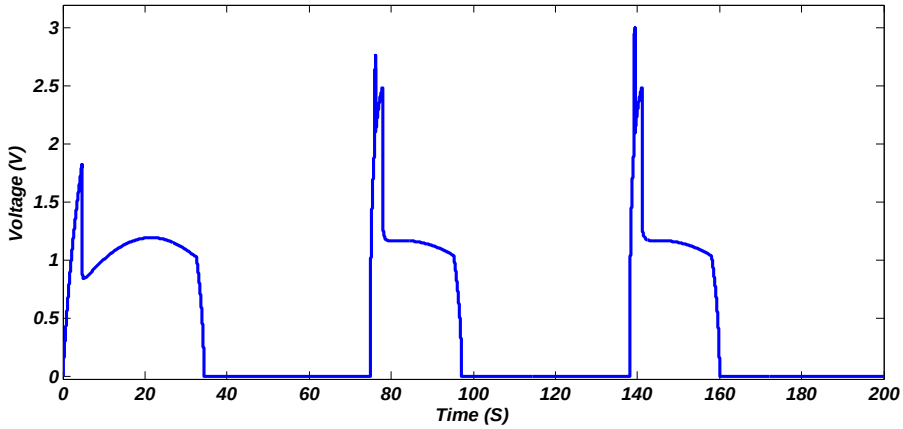

Figure 12. Input voltage for tracking sinusoidal input force with low frequency and large high variation in amplitude.

In this condition, during the upward of sinusoidal input force, the tracking is feasible, but because of low speed of cooling, the tracking is not achieved in the downward sinusoidal reference force. Moreover, because of high variation in amplitude, the acceptable tracking is not reachable. It should be also considered that SMAs has some hysteresis phenomena and thus some internal residual stress will remain. Therefore, the output force will never return to the initial condition at fixed length.

Figure 13 and Figure 14 depict another response for tracking control. In this case, the input frequency is high (1.20 Hz), but the amplitude of variation of the desired force is small (about 1N).

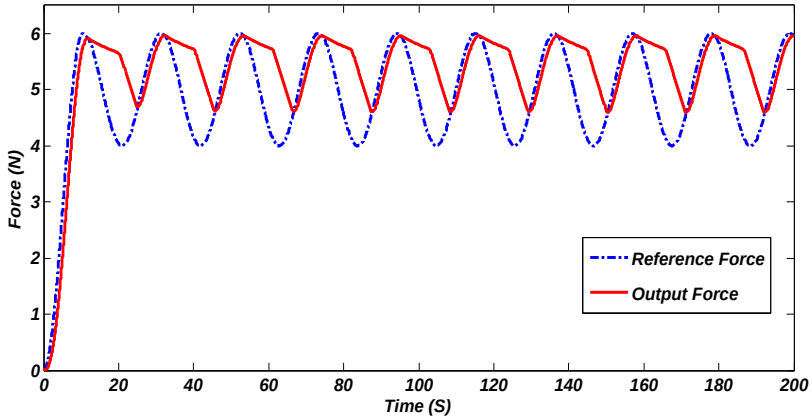

Figure 13. Tracking control for sinusoidal input force with high frequency and small variation in amplitude.

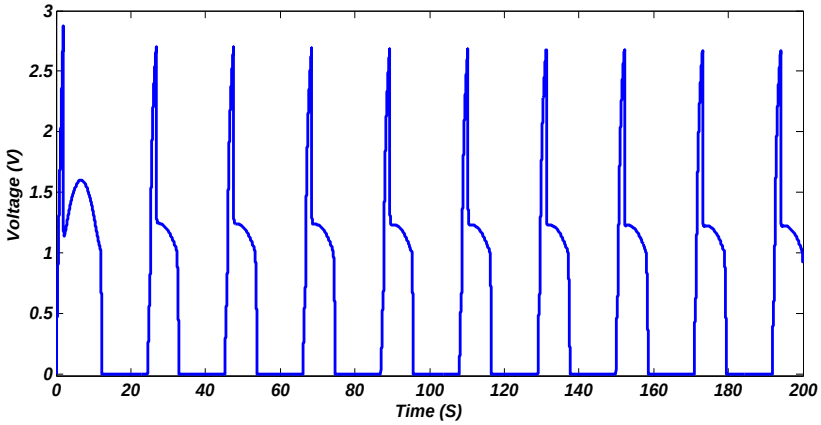

Figure 14. Input voltage for tracking sinusoidal input force with high frequency and small variation in amplitude.

As shown in Figure 13, in this case tracking is not possible because the frequency of the desired input is high. However, the satisfactory tracking is practicable to some extent while the input force is increasing. On the other hand, the tracking (in high frequency conditions) is not attainable while the force is decreasing due to the fact that SMA is cooled with a low speed.

In order to implement the proposed feedback linearization controller on the experimental set-up, the measurement of state-space variables is necessary. Since some of the state-space variables are immeasurable (ξ_s and ξ_T), a nonlinear observer is required to estimate these variables and evaluate experimental performance of the controller. This issue will be the future focus of this research.

VII. CONCLUSION

In this paper the procedures of state-space modeling and control of a micro actuator (shape memory alloy spring) is presented. The presented state-space model is a fundamental element in different aspects of MEMS such as micro robots and is well suited for control applications. To validate the proposed model, the open loop model is verified by some experimental tests. The results show good agreement between simulations and experimental tests which in turn confirm the accuracy of the state-space model. Based on input-output feedback linearization method, a nonlinear controller has been developed to control the output force of SMA spring actuators. As illustrated by simulations, the tracking is accessible in low frequency and small amplitude of variation of desired force. For high frequencies and amplitudes, the acceptable tracking will not be properly feasible. It should be considered that the SMA spring is cooled with a slow speed and as a result its response will be slow when the desired force decreases. Additionally, the hysteresis phenomenon causes a residual stress in SMA spring. Due to the fact that the output force could not be less than the produced residual force, the tracking is not possible when the amplitude of the desired force changes much. Thus, the satisfactory tracking depends on the frequency and amplitude of variation of the input signal.

REFERENCES

[1]. WangZ, Hang G, Li J, Wang Y, Xiao K. *A micro-robot fish with embedded SMA wire actuated flexible biomimetic fin.*Sensor Actuator A-Phys2008; 15; 354-360.

[2]. Kim B, Lee S, Park JH, Park JO. *Inchworm-like microrobot for capsule endoscope. In: IEEE 2004 Robotics and Biomimetics* Conference; 22-26 August 2004; Shenyang Marriott Hotel, Shenyang. China: IEEE. pp. 458-463.

[3]. Chang-Jun Q, Pei-Sun M, Qin Y. *A prototype micro-wheeled-robot using SMA actuator.* Sensor Actuator A-Phys 2004; 113;94-99.

[4]. Kim B, Lee MG, Lee YP, Kim Y, Lee G. *An earthworm-like micro robot using shape memory alloy actuator.* Sensor Actuator A-Phys 2006; 125; 429-437.

[5]. Holschuh B, Obropta E, Newman D. *Low spring index NiTi coil actuators for use in active compression garments.* IEEE-ASME T MECH 2015; 20; 1264-77.

[6]. Abiri R, Kabganian M, Nadafi R. *Fabrication, modeling and set-point control of a new flexible microrobot module (FMM) by using SMA actuators.* In: IEEE 2013 Robotics and Mechatronics Conference; 13–15February 2013; Tehran, Iran: IEEE. pp. 141-146.

[7]. Peng F, Jiang XX, Hu YR, Ng A. *Application of shape memory alloy actuators in active shape control of inflatable space structures.* In: IEEE 2005 Aerospace Conference; 4–15 March 2005; Big Sky, USA: IEEE. pp. 1-10.

[8]. Saadat S, Salichs J, Noori M, Hou Z, Davoodi H, Bar-On I, Suzuki Y, Masuda A. *An overview of vibration and seismic applications of NiTi shape memory alloy.* VTT SYMP 2002; 11:218-225.

[9]. Song G, Chaudhry V, Batur C. *Precision tracking control of shape memory alloy actuators using neural networks and a sliding-mode based robust controller.*VTT SYMP 2003; 12: 223-229.

[10]. Teh YH, Featherstone R. *Accurate force control and motion disturbance rejection for shape memory alloy actuators.* In: IEEE 2007 International Conference on Robotics and Automation; 10-14 April 2007; Roma, Italy: IEEE. pp. 4454-4459.

[11]. Moallem M, Lu J. *Application of shape memory alloy actuators for flexure control: theory and experiments.*IEEE-ASME T MECH2005;10:495-501.

[12]. Song G, Chaudhry V, Batur C. *Precision tracking control of shape memory alloy actuators using neural networks and a sliding-mode based robust controller.*VTT SYMP 2003; 12: 223-231.

[13]. Nguyen BK, Ahn KK. *Feedforward control of shape memory alloy actuators using fuzzy-based inverse Preisach model.*IEEE T CONTR SYST T 2009; 17:434-441.

[14]. Lei KF, Yam Y, Baranyi P. *Neural-fuzzy based control experiments on a shape memory alloy (SMA) positioning system.*In: IEEE 2001 American Control Conference; 10-14 June 2001; Arlington, USA: IEEE. pp. 3861-3865.

[15]. Kha NB, Ahn KK. *Position control of shape memory alloy actuators by using self-tuning fuzzy PID controller.* In: IEEE 2006 Industrial Electronics and Applications Conference; 24-27 May 2006; Singapore: IEEE. pp. 1-5.

[16]. Nguyen BK, Ahn KK. *Feedforward control of shape memory alloy actuators using fuzzy-based inverse Preisach model.*IEEE T CONTR SYST T 2009; 17: 434-41.

[17]. Kumon M, Mizumoto I, Iwai Z, Indou A. *Shape memory alloy actuator with simple adaptive control.* In: IEEE 2007 international conference oninnovativecomputing,information and control; 3-6 September 2007; Kumamoto: IEEE. pp. 429-432.

[18]. Bizdoaca NG, Petrisor A, Patrascu D, Pana C, Vasile C. *Mathematical model and conventional control for a shape memory alloy tendon actuated tentacle robot.* In: IEEE 2006 international conference on automation, quality and testing, robotics; 25-29 May 2006; Cluj-Napoca: IEEE. pp. 243-448.

[19]. Hadi A, Yousefi-Koma A, Moghaddam MM, Elahinia M, Ghazavi A. *Developing a novel SMA-actuated robotic module.*SENSOR ACTUAT A-PHYS 2010; 162; 72-81.

[20]. Brinson LC. *One-dimensional constitutive behavior of shape memory alloys: thermo mechanical derivation with non-constant material functions and redefined martensite internal variable.*J INTEL MAT SYST STR 1993; 4:229-242.

[21]. Liang C, Rogers CA. *Design of shape memory alloy springs with applications in vibration control.*J INTEL MAT SYST STR 1997; 8:314-322.

[22]. Aguiar RA, Savi MA, Pacheco PM. *Experimental and numerical investigations of shape memory alloy helical springs.*VTT SYMP 2010; 19: 127-138.
[23]. Kardan I, Abiri R, Kabganian M, Vahabi M. *Modeling of shape memory alloy springs using a recurrent neural network.*J THEOR APPL MECH 2013; 51: 711-718.